Title
A Deep Learning Approach to Automatic 3D Bone Shape Modeling From Clinical MRI

Author
Oeding, Jacob

Publication Date
2021

Peer reviewed|Thesis/dissertation

A Deep Learning Approach to Automatic 3D Bone Shape Modeling From Clinical MRI

by

Jacob Oeding

THESIS

Submitted in partial satisfaction of the requirements for degree of

MASTER OF SCIENCE

in

Biomedical Imaging

in the

GRADUATE DIVISION

of the

UNIVERSITY OF CALIFORNIA, SAN FRANCISCO

Approved:

DocuSigned by:

______________________________ Drew Lansdown

63B34698703149F...

Chair

DocuSigned by:

Valentina Pedoia ______________________________ Valentina Pedoia

DocuSigned by:

______________________________ Peder Larson

DocuSigned by:

Roland Krug ______________________________ Roland Krug

E4A4A067E4C8436...

____

Committee Members

Acknowledgements

Without the incredible help and support of my mentors Dr. Drew Lansdown and Dr. Valentina Pedoia, this work would not have been possible. I also want to thank Kenneth Gao and Francesco Caliva for their contributions to this project.

A Deep Learning Approach to Automatic 3D Bone Shape Modeling From Clinical MRI

Jacob F. Oeding

Abstract

Statistical shape modeling has been employed to study three-dimensional bony morphological features of the tibia and femur as potential risk factors for ACL injury and negative outcomes after ACL reconstruction. However, prior studies have been limited in size, largely due to the need for either CT imaging or high-resolution MRI with tedious manual segmentation. In this study, a deep learning model was trained to automatically segment tibia and femur bones from clinical MRI scans. The model was used to infer segmentations from a large dataset (> 300 images) of preoperative and postoperative clinical MR images from patients who had underwent ACL reconstruction and had clinical, two-dimensional PD-weighted MRIs. Three-dimensional bone shape models were constructed from inferred segmentations. PCA was performed, and results were compared between datasets of same knees imaged 6 months apart. Correlations between same knee principal components were moderate to strong, and point-to-point deviations between same knee vertices were small, indicating that reliable and repeatable statistical shape modeling can be obtained from clinical MRI sequences.

Table of Contents

List of Figures

List of Tables

Chapter 1: Introduction

Knee bony morphology is an important factor in surgical decision-making and surgical outcomes. Multiple bone shape features have been identified as risk factors for ACL injury and poor outcomes after ACL reconstruction (ACLR).(1) Thus, an accurate evaluation of tibiofemoral bone shape and anatomy may support improved preventative care, pre-operative planning, and post-surgical outcomes. For example, increased posterior femoral condylar depth is associated with higher failure rates in ACL reconstructed knees.(2) It has been proposed that the increased length of lateral and anterolateral knee structures during flexion and the increased relative laxity of these structures during extension — when most non-contact ACL injuries occur — result in increased rotational laxity that ultimately increases the risk for poor ACLR outcomes and reinjury.(3) Significant evidence suggests that the addition of lateral extra-articular tenodesis (LET) to ACLR results in improvements in rotational stability and better clinical outcomes compared with ACLR alone in high-risk patients.(4-6) Thus, identification of patients with bone shape features such as increased posterior femoral condyle depths could prove beneficial for surgical outcomes.

While three-dimensional reconstruction via computed tomography (CT) provides the current gold standard for measurement of complex bony shape structures, previous work has shown that high-resolution MRI with specialized sequences can produce 3D reconstructions similar to those produced from CT.(7) These MR imaging techniques have been used in prior studies to investigate tibiofemoral bone shape and its association with ACLR outcomes.(8-10) However, these techniques are not feasible for routine clinical use, as they require specialized sequences and extensive manual post-processing. As a result, the sizes of prior studies evaluating tibiofemoral bony morphology have been limited. Ideally, three-dimensional bone shape analysis could be automatically performed using readily available clinical MRIs from pre-operative and post-operative evaluations. Thus, the goal of this thesis is to develop a deep learning approach to produce automatic 3D bone shape models from 2D clinical MR images. As a result, the use of larger clinical datasets to more reliably characterize bony morphological characteristics associated with ACL injury is made possible.

Chapter 2: Methods

Clinical Data: MRI scans from 68 patients who had clinical, two-dimensional PD-weighted (3.5 mm slice thickness) knee MRI sequences were obtained from a previously acquired dataset. Diagnoses for all patients included ACL tears. Both contralateral and ipsilateral knees were imaged at three time points, one pre-operatively and two post-operatively.

Deep Learning Algorithm Development & Testing: To develop an automatic femur and tibia segmentation framework, a training and validation set split based on age, sex, BMI, and timing of scan (pre- or post-operative) was generated and used to train a deep convolutional neural network (CNN). Both pre-operative and post-surgical reconstruction scans were included in the dataset (22 pre-operative, 18 post-operative). The tibia and femur of each MRI was manually segmented with custom, in-house developed Matlab-based software. Twenty-eight of the manually segmented clinical, PD-weighted MRI volumes were selected to populate the training set, while six volumes were reserved for the validation set, which was used to evaluate the generalization capability of our machine learning system. The remaining six volumes were reserved for a test set, which was used to evaluate the final model performance.

Two separate deep learning models were trained, and information from each was used to construct a final volumetric segmentation to be used for the remainder of the shape modeling pipeline. One model was trained using only slices for which there was bone manually segmented on the ground truth. This was done to improve identification of the intricate details and shapes of the bone on slices for which there is bone and produce a more precise segmentation. A second model was trained on all slices of the MRI, regardless of whether bone was present, to improve the ability of our deep learning framework to identify whether bone is present on an image. For the model combining the two, if bone was determined to be present on an image using the second model, the first model was used to infer the segmentation.

Shape Modeling: Femur and tibia segmentations were inferred from the 2D images. Prior to inference, all 2D volumes were up-sampled to obtain a slice thickness of 0.5 mm. The resulting segmentations were used to produce 3D triangulated meshes using a Marching Cube algorithm.(11) Vertices of the triangulated meshes were then nonrigidly registered using FOCUSR, as described by Lombaert et al.(12)

Principal component analysis (PCA) was then performed to 1) simplify the complexity of the shape variation for analysis and 2) provide a means for evaluating the repeatability and reliability of our model. Via PCA, vertex coordinates were transformed to orthonormal bases. Each principle component (PC) mode was uncorrelated. The direction of maximum bone shape variance was indicated by the first PC, with each subsequent PC indicating the next most significant bone shape. Given the size of our dataset, 10 PCs were determined sufficient to capture most of the variance in each bone and provide appropriate validation when used to evaluate the repeatability of our model. A subset of 42 patients was selected and PCA was performed on two separate datasets of contralateral knee MRIs taken 6 months apart.

Statistical Analysis: To assess the repeatability of the SSM pipeline, correlations between corresponding PCs in each dataset were determined. Additionally, the average vertex-to-vertex distance between same knees at both timepoints was computed and compared with the average vertex-to-vertex distance between each knee and all other knees. Pearson's coefficients were computed and p-values generated to test the hypothesis of no correlation against the alternative hypothesis of a nonzero correlation. Significance was defined as $p < 0.05$.

Chapter 3: Results

Segmentation evaluation was conducted via the volumetric Dice Score Coefficient (DSC). **Table 1** shows the quantitative performance of each model on the separate test set of 6 MRI scans.

Table 1: *Model performance. The combined model uses the results of both the model trained on only slices manually segmented on the ground truth as well as the model trained on all slices regardless of whether a segmentation exists on the ground truth for a particular slice.*

Model	**DSC - Femur (%)**	**DSC - Tibia (%)**
All Slices	92.73 ± 2.16	92.90 ± 2.17
Only Segmented	91.87 ± 4.53	94.98 ± 1.36
Combined	95.29 ± 0.44	95.52 ± 0.75

The average DSC for the separate test set of 6 MRI scans was 95.29 ± 0.44 for the femur and 95.52 ± 0.75 for the tibia using the combined model. **Figure 1** displays a representative slice with automatic femur and tibia segmentations overlayed.

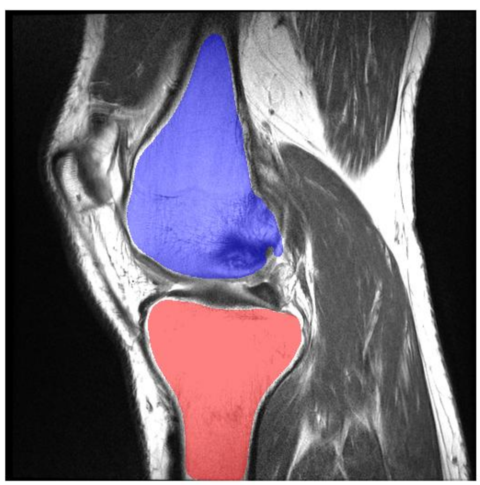

Figure 1: *DSC (%): 95.29 ± 0.44% (Femur), 95.52 ± 0.75% (Tibia).*

Table 2: *Correlation results from same knee multiple measurement PCA. Bolded values indicate $p < 0.05$.*

Femur/R	**1**	**2**	**3**	**4**	**5**	**6**	**7**	**8**	**9**	**10**
1	**0.936**	0.098	0.048	**0.333**	0.116	0.252	0.072	0.126	0.160	0.202
2	0.199	**0.668**	0.214	**0.316**	0.184	0.246	0.091	0.047	0.262	0.228
3	0.016	0.082	**0.413**	0.237	0.013	0.195	0.126	0.102	0.194	0.111
4	0.130	0.236	0.021	**0.563**	0.046	0.021	0.235	0.082	0.027	0.002
5	0.048	0.158	0.095	0.061	**0.792**	0.042	0.113	0.223	0.145	0.235
6	0.039	0.048	0.017	0.112	0.159	**0.474**	0.204	0.162	0.010	0.013
7	0.039	0.045	0.068	0.009	0.169	0.197	**0.415**	0.044	0.059	0.121
8	0.010	0.107	0.131	0.241	0.039	0.144	0.262	**0.673**	0.011	0.169
9	0.042	0.097	0.062	0.093	0.005	0.168	0.006	0.122	**0.550**	0.153
10	0.044	0.162	0.015	0.052	0.157	0.221	0.095	0.036	0.116	**0.425**
Tibia/R	**1**	**2**	**3**	**4**	**5**	**6**	**7**	**8**	**9**	**10**
1	**0.907**	0.199	**0.363**	0.194	**0.418**	0.269	**0.336**	0.249	0.167	0.032
2	0.096	**0.869**	0.200	0.062	0.153	0.028	0.054	0.037	0.085	0.097
3	0.099	0.221	**0.372**	0.268	0.044	0.135	0.067	0.148	0.192	0.252
4	0.027	0.139	0.291	**0.578**	0.004	0.015	0.090	0.046	0.139	0.064
5	0.184	0.019	0.020	0.008	**0.472**	0.011	0.055	0.022	0.009	**0.386**
6	0.047	0.013	0.134	0.111	0.047	**0.730**	**0.313**	0.056	0.159	0.295
7	0.111	0.089	0.127	0.105	0.207	0.194	**0.543**	0.140	0.300	0.064
8	0.006	0.088	0.127	0.075	0.150	0.064	0.303	**0.600**	0.195	0.096
9	0.006	0.033	0.068	0.078	0.024	0.177	**0.410**	0.028	**0.702**	0.106
10	0.113	0.175	0.037	0.057	0.021	0.146	0.206	0.026	0.074	**0.441**

PCA results are displayed in **Table 2**. All correlations between corresponding PCs measured from contralateral knees at both timepoints were moderate to strong and statistically significant, with R values ranging from 0.413-0.936 for the femur and 0.372-0.907 for the tibia, indicating good repeatability.

Among each of the 59,759 vertices describing the femur, the average same knee deviation of each vertex from the corresponding vertex at the second scan was 2.73 ± 1.69 mm. For the tibia, the average same knee deviation of each of the 36,679 vertices was 2.41 ± 1.37 mm. When each knee was measured against all other knees in the dataset, average deviations of 5.61 ± 0.95 mm and 6.22 ± 1.05 mm were obtained for the femur and tibia, respectively. These results are shown in **Figure 2**.

For a qualitative comparison, **Figure 3** shows representative fully automatic reconstructions of a single patient's femur and tibia from clinical MRI scans obtained 6 months apart.

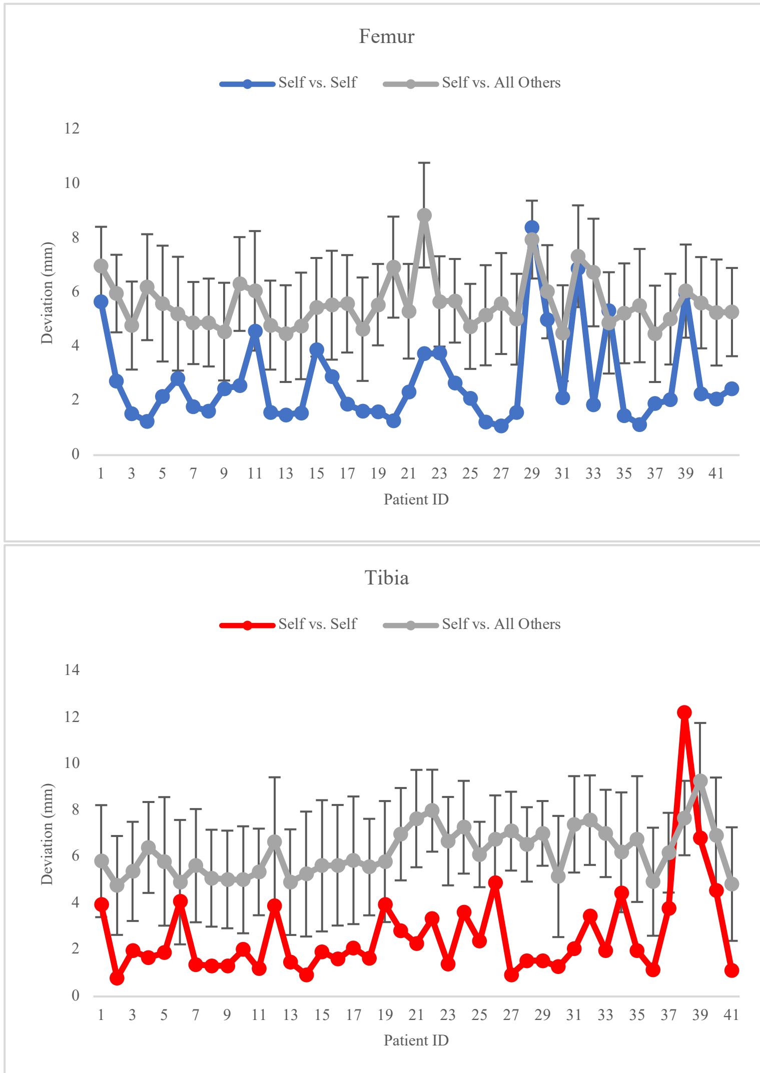

Figure 2: *Comparison of deviations of mesh vertices from same knee and all other knees imaged 6 months apart.*

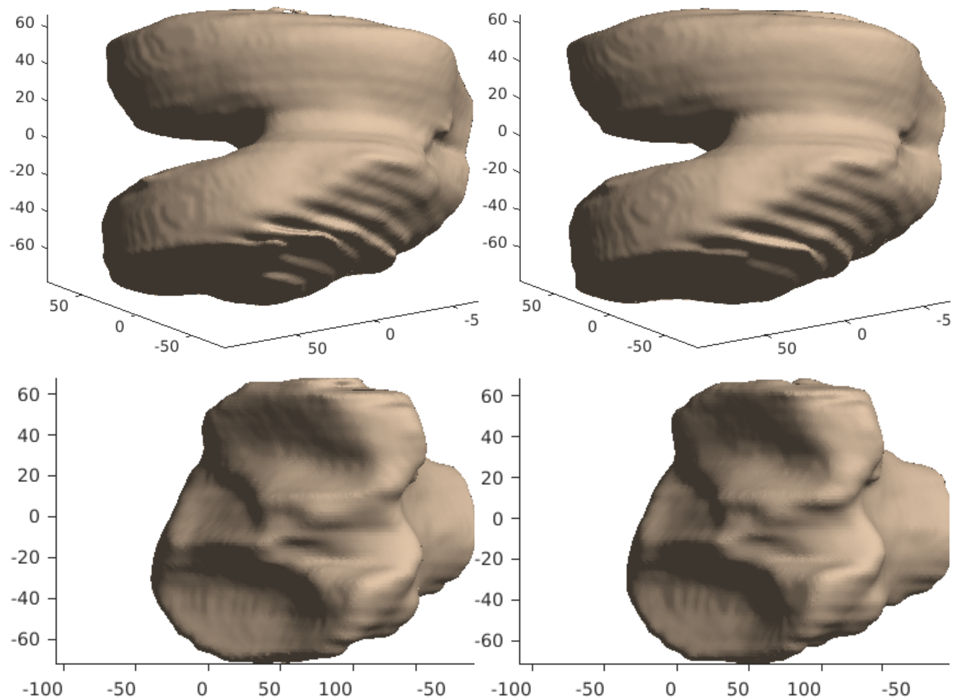

Figure 3: *Qualitative comparison between clinical MRI-based 3D reconstructions at baseline (left) and follow-up (right).*

Chapter 4: Discussion

This study presents a fully automatic, deep learning-based strategy for extracting tibiofemoral bone shape from clinical MRI scans. The methodology presented herein enables the use of clinical MRI for 3D SSM, providing for large-scale studies with the potential to discover new associations between bony morphology, injury risk, and outcomes for knee conditions such as ACL tears.

Excellent segmentation performance and reliable PCA was demonstrated using a deep learning model and statistical shape modeling pipeline on clinical MRI scans. Between the two datasets of contralateral knee MRIs taken at separate post-operative timepoints, the model was able to reliably and repeatably determine the shape variants most significant among our cohort of 42 patients, as indicated by moderate to strong correlations among PCs. Additionally, significantly small deviations in vertex-to-vertex distances between corresponding 3D reconstructions were observed for same knees measured 6 months apart. Further studies will validate these measurements relative to CT or high-resolution MRI.

References

1. Bayer S, Meredith SJ, Wilson KW, de Sa D, Pauyo T, Byrne K, et al. Knee Morphological Risk Factors for Anterior Cruciate Ligament Injury: A Systematic Review. J Bone Joint Surg Am. 2020;102(8):703-18.

2. Grassi A, Macchiarola L, Urrizola Barrientos F, Zicaro JP, Costa Paz M, Adravanti P, et al. Steep Posterior Tibial Slope, Anterior Tibial Subluxation, Deep Posterior Lateral Femoral Condyle, and Meniscal Deficiency Are Common Findings in Multiple Anterior Cruciate Ligament Failures: An MRI Case-Control Study. Am J Sports Med. 2019;47(2):285-95.

3. Pfeiffer TR, Burnham JM, Hughes JD, Kanakamedala AC, Herbst E, Popchak A, et al. An Increased Lateral Femoral Condyle Ratio Is a Risk Factor for Anterior Cruciate Ligament Injury. J Bone Joint Surg Am. 2018;100(10):857-64.

4. Grassi A, Zicaro JP, Costa-Paz M, Samuelsson K, Wilson A, Zaffagnini S, et al. Good mid-term outcomes and low rates of residual rotatory laxity, complications and failures after revision anterior cruciate ligament reconstruction (ACL) and lateral extra-articular tenodesis (LET). Knee Surg Sports Traumatol Arthrosc. 2020;28(2):418-31.

5. Ahn JH, Kim J, Mun JW. A Retrospective Comparison of Single-Bundle Anterior Cruciate Ligament Reconstruction With Lateral Extra-Articular Tenodesis With Double-Bundle Anterior Cruciate Ligament Reconstruction. Arthroscopy. 2021;37(3):976-84.

6. Hewison CE, Tran MN, Kaniki N, Remtulla A, Bryant D, Getgood AM. Lateral Extra-articular Tenodesis Reduces Rotational Laxity When Combined With Anterior Cruciate Ligament Reconstruction: A Systematic Review of the Literature. Arthroscopy. 2015;31(10):2022-34.

7. Lansdown DA, Cvetanovich GL, Verma NN, Cole BJ, Bach BR, Nicholson G, et al. Automated 3-Dimensional Magnetic Resonance Imaging Allows for Accurate Evaluation of Glenoid Bone Loss Compared With 3-Dimensional Computed Tomography. Arthroscopy. 2019;35(3):734-40.

8. Lansdown DA, Pedoia V, Zaid M, Amano K, Souza RB, Li X, et al. Variations in Knee Kinematics After ACL Injury and After Reconstruction Are Correlated With Bone Shape Differences. Clin Orthop Relat Res. 2017;475(10):2427-35.

9. Zhong Q, Pedoia V, Tanaka M, Neumann J, Link TM, Ma B, et al. 3D bone-shape changes and their correlations with cartilage T1ρ and T2 relaxation times and patient-reported outcomes over 3-years after ACL reconstruction. Osteoarthritis Cartilage. 2019;27(6):915-21.

10. Pedoia V, Su F, Amano K, Li Q, McCulloch CE, Souza RB, et al. Analysis of the articular cartilage T. J Orthop Res. 2017;35(3):707-17.

11. Lorensen WE, Cline HE. Marching cubes: a high resolution 3D surface construction algorithm. SIGGRAPH '87: Proceedings of the 14th annual conference on computer graphics and interactive technique; 1987.

12. Lombaert H, Grady L, Polimeni JR, Chereit F. FOCUSR: feature oriented correspondence using spectral regularization—A method for precise surface matching. IEEE Trans Pattern Anal Mach Intell. 2013; 35(9):2143-2160.

Publishing Agreement

It is the policy of the University to encourage open access and broad distribution of all theses, dissertations, and manuscripts. The Graduate Division will facilitate the distribution of UCSF theses, dissertations, and manuscripts to the UCSF Library for open access and distribution. UCSF will make such theses, dissertations, and manuscripts accessible to the public and will take reasonable steps to preserve these works in perpetuity.

I hereby grant the non-exclusive, perpetual right to The Regents of the University of California to reproduce, publicly display, distribute, preserve, and publish copies of my thesis, dissertation, or manuscript in any form or media, now existing or later derived, including access online for teaching, research, and public service purposes.

DocuSigned by:

Jacob F Oeding

FED631D614CE483... Author Signature

9/2/2021

Date